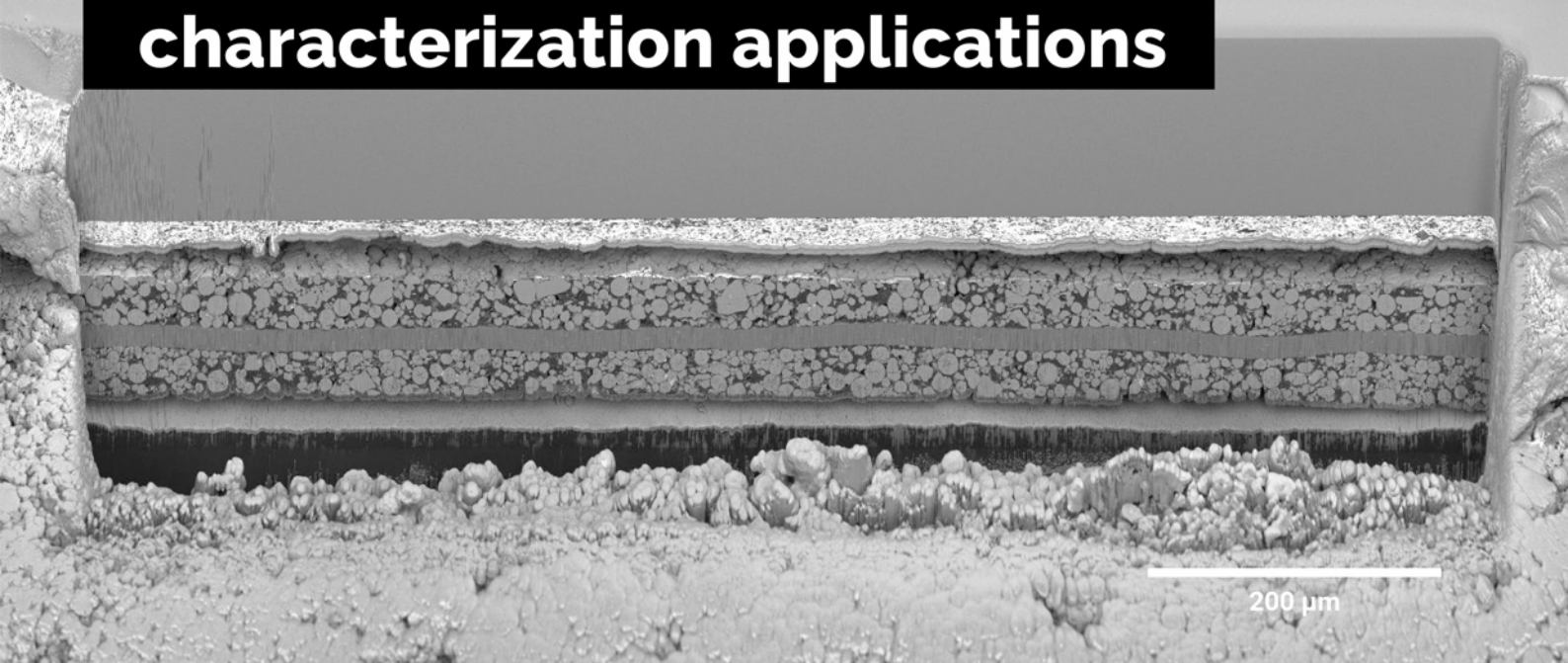


# A unique combination of Plasma FIB and field-free UHR SEM for the widest range of multiscale materials characterization applications



1 mm cross-section through a Li-ion battery electrode

## TESCAN AMBER X

- ✓ High throughput, large area FIB milling up to 1 mm
- ✓ Ga-free microsample preparation
- ✓ Ultra-high resolution, field-free FE-SEM imaging and analysis
- ✓ In-column SE and BSE detection
- ✓ Spot optimization for high-throughput, multi-modal FIB-SEM tomography
- ✓ Superior field of view for easy navigation
- ✓ Essence™ easy-to-use, modular graphical user interface



For more information visit

[www.tescan.com](http://www.tescan.com)

# Highly Transparent, Scalable, and Stable Perovskite Solar Cells with Minimal Aesthetic Compromise

Tianran Liu, Xiaoming Zhao,\* Ping Wang, Quinn C. Burlingame, Junnan Hu, Kwangdong Roh, Zhaojian Xu, Barry P. Rand, Minjie Chen, and Yueh-Lin Loo\*

Transparent photovoltaics (TPVs) can be integrated into the surfaces of buildings and vehicles to provide point-of-use power without impacting aesthetics. Unlike TPVs that target the photon-rich near-infrared portion of the solar spectrum, TPVs that harvest ultraviolet (UV) photons can have significantly higher transparency and color neutrality, offering a superior solution for low-power electronics with stringent aesthetic tolerance. In addition to being highly transparent and colorless, an ideal UV-absorbing TPV should also be operationally stable and scalable over large areas while still outputting sufficient power for its specified application. None of today's TPVs meet all these criteria simultaneously. Here, the first UV-absorbing TPV is demonstrated that satisfies all four criteria by using CsPbCl<sub>2.5</sub>Br<sub>0.5</sub> as the absorber. By precisely tuning the halide ratio during thermal co-evaporation, high-quality large-area perovskite films can be accessed with an ideal absorption cutoff for aesthetic performance. The resulting TPVs exhibit a record average visible transmittance of 84.6% and a color rendering index of 96.5, while maintaining an output power density of 11 W m<sup>-2</sup> under one-sun illumination. Further, the large-area prototypes up to 25 cm<sup>2</sup> are demonstrated, that are operationally stable with extrapolated lifetimes of >20 yrs under outdoor conditions.

on strong absorption of near-infrared (NIR) wavelengths with semitransparency to visible wavelengths, ultraviolet (UV)-absorbing devices are gaining traction due to their intrinsic potential for higher transparency and color neutrality.<sup>[2]</sup> These benefits make them an ideal match for low-power applications that prioritize aesthetics, such as power sources for internet-of-things sensors, heads-up displays (HUDs), and electrochromic windows (ECWs) that can adaptively control visual comfort and solar heat gain.<sup>[1,3-7]</sup>

Several candidate UV-harvesting material systems for TPVs have been demonstrated, including small-molecule organics, metal oxides, metal halide salts, and organic-inorganic hybrid perovskites.<sup>[3,8-17]</sup> However, none of these materials have demonstrated compatibility with the full slate of stringent requirements for practical TPV applications—excellent aesthetics while still outputting sufficient power for a given application, long-term

operational stability, and scalability of both device fabrication and device area.<sup>[1]</sup> As of the writing of this manuscript, no UV-harvesting solar cells have shown extended stability ( $T_{80} > 3000$  h) or scalability (>2 cm<sup>2</sup>),<sup>[1,17]</sup> with only a handful of UV-absorbers having demonstrated compatibility with transparent top electrode deposition.<sup>[8,10-16]</sup> Of devices with transparent electrodes, the optical properties of most are well below the intrinsic aesthetic limits for UV-absorbing TPVs, with some suffering from high haze, and others from low transparency or yellow tinting.<sup>[11,13,14,16]</sup> Of the few color-neutral UV-absorbing solar cells with low haze, either their average visible transmittance (AVT) is limited (<70%),<sup>[10]</sup> or their power-conversion efficiencies (PCEs) are less than 0.7%,<sup>[8,10,12,15]</sup> highlighting the challenges associated with realizing photovoltaics that simultaneously approaches the aesthetic and power output potential of UV-harvesting TPVs.

Here, we demonstrate the use of cesium lead halide inorganic perovskites as active layers in highly transparent, stable, and scalable solar cells. By employing thermal evaporation, we avoid the limitations of precursor solubility to access a unique perovskite composition that is scalable, structurally uniform, thick, and sufficiently robust to survive the deposition of sputtered indium tin oxide (ITO) top electrodes. By tuning the halide ratio during deposition, we achieve a perovskite film with an absorption cutoff of 435 nm, which is ideal for

## 1. Introduction

Transparent photovoltaics (TPVs) are rapidly emerging as a promising solution to electrify glass surfaces on buildings and vehicles.<sup>[1]</sup> Though TPV development has mostly focused


T. Liu, X. Zhao, Y.-L. Loo  
Department of Chemical and Biological Engineering  
Princeton University  
New Jersey 08544, USA

E-mail: xz11@princeton.edu; lloo@princeton.edu

T. Liu, P. Wang, J. Hu, K. Roh, Z. Xu, B. P. Rand, M. Chen  
Department of Electrical Engineering  
Princeton University  
New Jersey 08544, USA

P. Wang, Q. C. Burlingame, B. P. Rand, M. Chen  
Andlinger Center for Energy and the Environment  
Princeton University  
Princeton, New Jersey 08544, USA

K. Roh  
Department of Physics  
Ewha Womans University  
Seoul 03760, Republic of Korea

 The ORCID identification number(s) for the author(s) of this article can be found under <https://doi.org/10.1002/aenm.202200402>.

DOI: 10.1002/aenm.202200402

maximizing color neutrality and transparency.<sup>[18]</sup> Employing these active layers, we demonstrate functional TPVs, complete with transparent electrodes, that exhibit a record high AVT of 84.6% with a near-perfect color rendering index (CRI) of 96.5 in the absence of any anti-reflective coating and prior to subtracting the reflection from glass. In addition to this superior aesthetic performance, our TPVs produce a power density of  $11 \text{ W m}^{-2}$  (PCE = 1.1%) under simulated AM1.5G illumination. Importantly, our encapsulated Cs-based inorganic perovskite TPVs also experience a mere 3.5% PCE loss after operating at their maximum power point (MPP) under continuous simulated one-sun illumination for over 1100 h, resulting in an extrapolated lifetime of over 20 yr. Finally, we have successfully extended lab-scale prototypes to large-area devices with active areas up to  $25 \text{ cm}^2$ , representing the largest transparent solar cells (AVT > 60%) reported in the scientific literature to-date.

## 2. Results and Discussions

To identify the optimal absorption cutoff for TPVs that maximizes AVT and CRI, we calculated the theoretical optical performance metrics, theoretical photocurrent, and PCE limit of a step-function absorber with various cutoff wavelengths using the method described by Lunt,<sup>[18]</sup> as shown in Figure 1a and Figure S1, Supporting Information. Reflection and parasitic absorption were not considered in this simplified calculation.<sup>[19–21]</sup> While absorbers with a cutoff wavelength of <435 nm produce less current than an absorber with a 435 nm cutoff, their potential aesthetic benefits are limited to an AVT increase of <1% and a CRI increase of <4%. Despite their higher power output potential, the CRI for absorbers with an absorption cutoff >435 nm drops precipitously due to the

orange/yellow tint they acquire from absorbing blue light. Thus here, we target an absorption cutoff of 435 nm to maximize the aesthetic performance of the solar cells without unnecessarily sacrificing photocurrent.<sup>[15,18]</sup>

To engineer an absorber that meets this criterion, we first fabricated  $\text{CsPbCl}_3$  films by thermal evaporation to circumvent the poor solubility of CsCl (Figure S2, Supporting Information),<sup>[15,22]</sup> and to avoid the use of environmentally harmful solvents.<sup>[23–27]</sup> Inorganic perovskites, in the absence of any mobile/volatile components, have shown promising stability against thermal and light stresses,<sup>[28–30]</sup> and  $\text{CsPbCl}_3$  has a bandgap of 3.0 eV corresponding to an absorption cutoff and a photoluminescence peak of 415 nm, as shown in Figure 1b, which makes it a promising UV-absorber starting point.<sup>[22]</sup> In order to shift absorption toward a cutoff of 435 nm, we evaporated films with increasing amounts of CsBr, until the ideal stoichiometry was identified at  $\text{CsPbCl}_{2.5}\text{Br}_{0.5}$ , with the absorption spectrum shown in Figure 1b. We observe that Br- inclusion forms a pure  $\text{CsPbCl}_{2.5}\text{Br}_{0.5}$  cubic phase with a slightly expanded lattice, as evidenced by the cubic (011) reflection shift from  $2\theta = 22.4^\circ$  to  $22.2^\circ$  shown in Figure 1c. The  $\text{CsPbCl}_{2.5}\text{Br}_{0.5}$  films also appear to form larger grains than  $\text{CsPbCl}_3$  films, as evidenced by a decrease in the full width at half maximum of this reflection from  $0.47^\circ$  to  $0.32^\circ$ , corresponding to an increase in correlation length from  $18.1 \pm 0.8$  to  $26.4 \pm 0.9$  nm (Figure S3, Supporting Information).<sup>[31–34]</sup> This assertion is consistent with the increase in grain size seen in the scanning electron microscopy (SEM) image of  $\text{CsPbCl}_{2.5}\text{Br}_{0.5}$  shown in Figure 1d.<sup>[35,36]</sup> Increasing the Br/Cl ratio beyond 0.5/2.5 resulted in yellow films that decreases aesthetic performance, as shown in the inset of Figure 1a for a  $\text{CsPbCl}_2\text{Br}$  film; additional characterization of the  $\text{CsPbCl}_2\text{Br}$  film is summarized in Figure S4, Supporting Information.

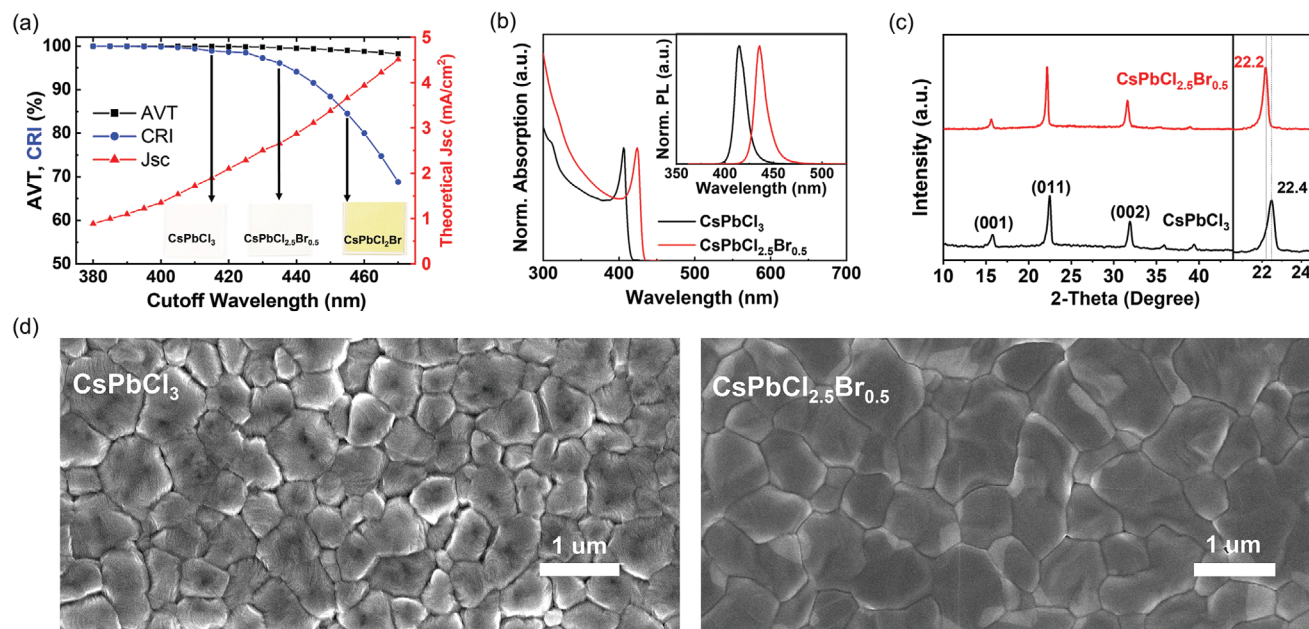


**Figure 1.** Structural and optical properties of  $\text{CsPbCl}_x\text{Br}_{3-x}$  perovskite. a) Calculated average visible transmittance (AVT), color rendering index (CRI), and theoretical photocurrent density limit as a function of the absorption cutoff wavelength of an absorber with the photographs of  $\text{CsPbCl}_x\text{Br}_{3-x}$  films (as inset). b) Absorption spectra and steady-state photoluminescence spectra (as inset), c) X-ray diffraction patterns, and d) scanning electron microscopy images of ultraviolet (UV)-absorbing  $\text{CsPbCl}_x\text{Br}_{3-x}$  perovskite films.



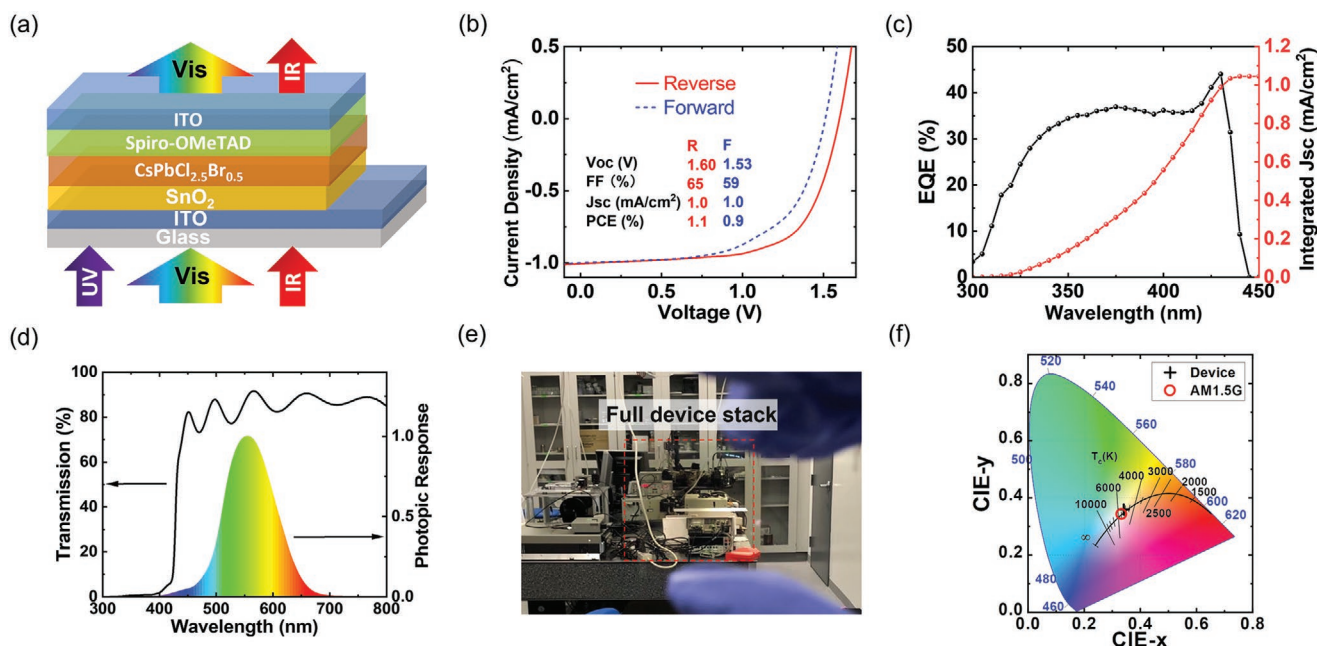


**Figure 2.** Device characterization of  $\text{CsPbCl}_{2.5}\text{Br}_{0.5}$  transparent photovoltaics (TPVs). a) Scheme of device structure of  $\text{CsPbCl}_{2.5}\text{Br}_{0.5}$  transparent solar cells. b) Current density-voltage ( $J$ - $V$ ) characteristics under forward and reverse voltage scan of TPVs based on  $\text{CsPbCl}_{2.5}\text{Br}_{0.5}$ . c) External quantum efficiency (EQE) of the TPV. d) Transmittance spectrum of a  $\text{CsPbCl}_{2.5}\text{Br}_{0.5}$  TPV with the photopic response of the human eye is shown for reference. e) A photograph taken through a  $1 \text{ cm}^2$  full device stack. f) Color coordinates of the TPV device and AM 1.5G on the CIE 1931 chromaticity diagram.

To study the photovoltaic performance of solar cells based on thermally-evaporated  $\text{CsPbCl}_{2.5}\text{Br}_{0.5}$  films, we first fabricated non-transparent devices with the conventional architecture shown in the inset of Figure S5a, Supporting Information. Representative current density-voltage ( $J$ - $V$ ) curves with device performance parameters and external quantum efficiency (EQE) spectra are shown in Figure S5, Supporting Information. The champion device produces an output power density of up to  $15 \text{ W m}^{-2}$  (PCE = 1.5%), with an open-circuit voltage ( $V_{OC}$ ) of 1.77 V and a fill factor (FF) of 75% under simulated AM1.5G solar illumination. To the best of our knowledge, this  $V_{OC}$  is the highest among perovskite solar cells,<sup>[37]</sup> surpassing those of devices comprising absorbers with comparable bandgaps based on solution-processed  $\text{MAPbCl}_x\text{Br}_{3-x}$ .<sup>[15]</sup>

We further fabricated TPVs based on  $\text{CsPbCl}_{2.5}\text{Br}_{0.5}$  in a device structure comprising ITO/ $\text{SnO}_2$ /perovskite/ $2,2'',7,7''$ -Tetrakis[N,N-di(4-methoxyphenyl)amino]-9,9'-spirobifluorene (Spiro-OMeTAD)/ITO, as shown in Figure 2a. In contrast to semi-transparent metal electrodes, such as silver, gold, and aluminum, ITO is more transparent across the visible and near-IR range.<sup>[38,39]</sup> This high transparency and color neutrality make it ideal for TPVs, especially UV-absorbing TPVs that prioritize aesthetics. Sputtering of ITO is notorious for causing damage to the underlying layers. Such damage is frequently characterized by shunting and/or reduced fabrication yields of solar cells,<sup>[40,41]</sup> as well as the formation of a so-called "S-kink" in the  $J$ - $V$  curves.<sup>[21,42-44]</sup> Here, we employ a low-power sputtering process to deposit ITO atop a thick (130 nm) spiro-OMeTAD hole transport layer. Our fabrication yields are consistently high (95%) and these devices do not exhibit any observable sputtering damage in cross-sectional SEM images (Figure S6, Supporting Information), implying that the thick ( $\approx 400 \text{ nm}$ ) and

uniform, pinhole-free inorganic perovskite films we employ here are sufficiently robust to resist sputtering damage. We summarize the photovoltaic performance of TPVs based on  $\text{CsPbCl}_{2.5}\text{Br}_{0.5}$  in Figure S7 and Table S2, Supporting Information, and show a representative  $J$ - $V$  curve and EQE spectrum in Figure 2b,c, respectively; the stabilized output characteristics are shown in Figure S8, Supporting Information. We note that the 400 nm thick perovskite layer is sufficiently thick to absorb nearly all UV/near-UV photons in the absence of a reflective metal electrode, leading to comparable  $J_{SC}$  in these devices compared to their opaque counterparts.

We show the transmittance and reflectance of a full-stack, functional TPV with this same device structure in Figure 2d and Figure S9, Supporting Information, respectively, and a photograph of the full-stack device is shown in Figure 2e. As with the  $\text{CsPbCl}_{2.5}\text{Br}_{0.5}$  perovskite film, the TPV stack exhibits a sharp absorption cutoff at around 435 nm because of the interfacial layers and electrodes employed in this device stack are also visibly transparent.<sup>[38,45-48]</sup> Despite the absence of an anti-reflection coating, the transparent device exhibits a record high AVT of 84.6%, and a near-perfect CRI of 96.5. Figure 2f shows the Commission Internationale d'Éclairage (CIE) 1931 chromaticity coordinates of sunlight transmitted through the perovskite TPV [0.34, 0.36] and of AM1.5G sunlight [0.33, 0.34] for comparison. Given the proximity of the TPV's chromaticity coordinates to those of AM1.5G sunlight, the TPV is effectively colorless and comparable in both transparency and color neutrality to uncoated glass.<sup>[1]</sup> In addition, unlike previous perovskite films that incorporate  $\text{Cl}^-$ , which exhibit significant haze,<sup>[15]</sup> the absorbers and devices in this work have virtually no haze due to the uniformity and homogeneity of the morphology that is typical of thermally-evaporated films. The haze ratio of

our TPV is <0.5% over the spectrum as shown in Figure S10, Supporting Information.

Since there is an inherent tradeoff between power generation and transparency in TPVs, direct comparison of TPV performance should be done with potential applications in mind. While the light utilization efficiency ( $LUE = AVT \times PCE$ ) is a commonly used metric to compare TPVs, it gives equal weight to efficiency and transparency. LUE thus does not properly ascribe value for TPVs that prioritize color neutrality and high transparency, such as those detailed in this work. Thus, to contextualize the performance of our cells, we compared them to other high-transparency devices—both those targeting UV wavelengths and those that absorb NIR light with  $AVT > 60\%$ , as shown in Table S1, Supporting Information. Although some devices in the literature approach or exceed the 1.1% PCE of our TPVs because they absorb increasing amounts of blue light, this enhanced efficiency comes at the expense of aesthetic performance, as illustrated in Figure 1a for a  $CsPbCl_2Br$  film.

Another important aspect to consider for TPV technology is device stability, which should be >25 yr for window-integrated applications.<sup>[1]</sup> Here, we subjected encapsulated  $CsPbCl_{2.5}Br_{0.5}$  TPVs to continuous aging under simulated solar illumination (Figure S11, Supporting Information) and tracked their MPP with time according to the International Summit on Organic and Hybrid Photovoltaic Stability protocol ISOS-L-1I.<sup>[49]</sup> As shown in Figure 3a, we observe a mere 3.5% reduction in PCE after 1100 h of aging, which linearly extrapolates to a  $T_{80}$  lifetime of >6500 h.<sup>[17,50,51]</sup> When we consider that an average of 850 W-h  $m^{-2}$  of sunlight is received on a vertical surface in Princeton, New Jersey, USA per day according to the National Solar Irradiation Database, this lifetime translates to more than 20 yr of outdoor operation.<sup>[17,52]</sup> As shown in Figure 3b, we also studied the extreme moisture and thermal stabilities of unencapsulated  $CsPbCl_{2.5}Br_{0.5}$ -based TPVs with CuSCN as a hole transport material in humid air ( $\approx 70\%$  RH, room temperature) and at a high temperature (85 °C). The photovoltaic and aesthetic performance of these devices are shown in Figure S12, Supporting Information. Our TPV shows less than 10% degradation after 500 h of aging in both cases, consistent with previous reports of high stability  $CsPbCl_3$  and  $CsPbBr_3$ -based optoelectronic devices.<sup>[53–58]</sup>

In addition to efficiency, aesthetics, and stability; large-area scalability is critical to realizing fully practical TPVs. Figure 4a shows representative  $J-V$  characteristics of a TPV cell with a 1.2  $cm^2$  active area. Its performance is comparable to that of the 0.09  $cm^2$  TPV, as tabulated in Table S3, Supporting Information. We also fabricated TPVs with areas of 10 and 25  $cm^2$ ; their performance parameters are summarized in Figure S13 and Table S3, Supporting Information. Almost all TPVs reported thus far have active areas that are approximately 0.1  $cm^2$ , with only a few publications reporting TPVs that are 1  $cm^2$  or greater, as shown in Table S1, Supporting Information. At 25  $cm^2$ , our TPV is an order of magnitude larger in the area compared to the largest device area (1.5  $cm^2$ ) reported prior to this work.<sup>[59]</sup> While the photovoltaic performance of our 1.2  $cm^2$  TPVs is nearly identical to that of the smaller 0.09  $cm^2$  TPVs, both FF and  $J_{SC}$  decrease with further increases in device areas (10 and 25  $cm^2$ ), as shown in Figure S13 and Table S3, Supporting Information. These losses are attributed to the performance being increasingly limited by the series resistance of the ITO top electrode and nonuniformity of spin-coated spiro-OMeTAD hole transport layer over larger areas.<sup>[60]</sup> Figure 4b shows a photograph of a 25  $cm^2$  TPV operating outdoors, demonstrating its transparency and color neutrality. To demonstrate the utility of UV-absorbing TPVs, we show that our large area (25  $cm^2$ ) devices can readily power an ECW (Figure S14a–c, Supporting Information), an HUD (Figure S14d, Supporting Information), and light-emitting diodes (LEDs) (Figure S14e, Supporting Information) while operating outdoors under ambient lighting, as shown in Figure S14, Supporting Information, with sufficient power overhead to trickle charge an energy storage element to continue operation during periods of solar intermittency.

### 3. Conclusion

An ideal UV-absorbing TPV should be highly transparent, colorless, operationally stable, and scalable over large areas. Here, we demonstrate TPVs that meet each of these criteria by using inorganic  $CsPbCl_{2.5}Br_{0.5}$  as the absorber. To circumvent the low solubility of Cl-based perovskite precursors, we employed thermal co-evaporation of CsCl, CsBr, and PbCl<sub>2</sub>

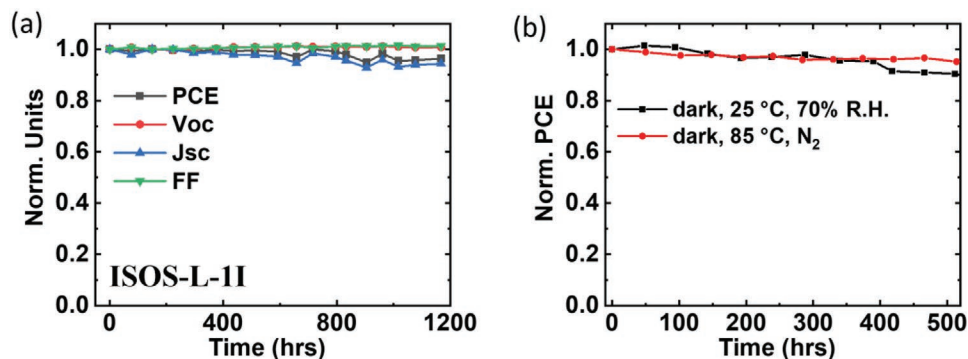


**Figure 3.** Stability of  $CsPbCl_{2.5}Br_{0.5}$  TPVs. a) Normalized power-conversion efficiency (PCE) for an encapsulated  $CsPbCl_{2.5}Br_{0.5}$  TPV operating at maximum power point (MPP) under continuous simulated one-sun illumination at ambient conditions (about 40 °C, 40% R.H.), tested according to ISOS-L-1I protocol. b) Normalized PCE over time for unencapsulated solar cells based on  $CsPbCl_{2.5}Br_{0.5}$  with CuSCN as a hole transport layer. The aging conditions are  $\approx 70\%$  R.H. air and  $\approx 25$  °C in the dark and  $\approx 85$  °C in inert atmosphere in the dark.

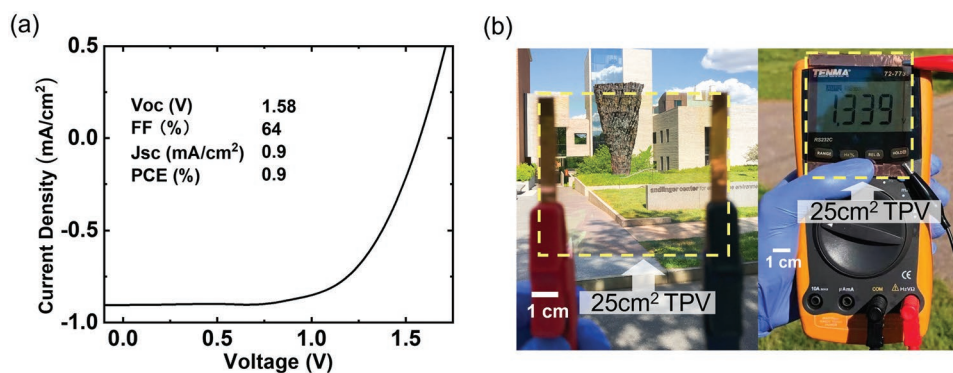


**Figure 4.** Area scaling of CsPbCl<sub>2.5</sub>Br<sub>0.5</sub> TPVs. a)  $J$ - $V$  characteristics of a 1.2 cm<sup>2</sup> TPV. b) Photographs taken outdoors of a 25 cm<sup>2</sup> TPV and its photovoltage shown on a multimeter under sunlight.

precursors, which yielded high-quality, large-area films that resist sputtering damage during ITO top electrode deposition. The resulting TPVs leverage absorbers with the optimal absorption cutoff for maximum transparency (435 nm), allowing us to achieve a record AVT of 84.6% and a near-perfect CRI of 96.5 with virtually no haze. In addition to their excellent optical performance, the TPVs are highly stable with extrapolated lifetimes >20 yr operating outdoors and readily scale to areas of 25 cm<sup>2</sup>. This work demonstrates the potential of these unique UV-absorbing TPVs as candidates for future see-through solar cell technologies, which can be applied on transparent surfaces for power generation with minimal aesthetic compromise.

#### 4. Experimental Section

**Materials:** PbCl<sub>2</sub> (99.99%) was purchased from TCI America. CsCl (99.999%), CsBr (99.999%), 4-tert-butylpyridine (t-BP) (98%), diethyl sulfide (98%), and CuSCN (>99%) were purchased from Sigma-Aldrich. SnO<sub>2</sub> dispersion (15 wt% in H<sub>2</sub>O) was purchased from Alfa Aesar. Chlorobenzene (>99.8%) was purchased from Acros Organics. Spiro-OMeTAD (>99%) was purchased from 1-Material. Bis(trifluoromethane) sulfonimide lithium salt (Li-TFSI) (99.95%) was purchased from Yingkou Libra Technology. All chemicals were used as received without further purification. Solar cell substrates were prepatterned indium-ITO glass obtained from Yingkou Advanced Election Technology Co., Ltd.

**Perovskite Thin film Deposition:** The perovskite layer was deposited by thermally co-evaporating CsCl, CsBr, and PbCl<sub>2</sub> from different sources in vacuum (< 3 × 10<sup>-6</sup> mbar) with an evaporation rate of 5 Å s<sup>-1</sup>. The molar ratio of CsCl, CsBr, and PbCl<sub>2</sub> was adjusted from 1:0:1, 1:1:2 to 0:1:1 for CsPbCl<sub>3</sub>, CsPbCl<sub>2.5</sub>Br<sub>0.5</sub> and CsPbCl<sub>2</sub>Br perovskite films, respectively. After co-evaporation, the samples were transferred to a nitrogen glovebox and annealed at 150 °C for 10 min.

**Characterizations:** UV-vis absorption, transmission, and reflection spectra were obtained on an Agilent Technologies Cary 5000 spectrophotometer. Steady-state photoluminescence was measured with a high-resolution spectrometer (Princeton Instruments, Spectra Pro HRS-3000). X-ray diffraction measurements were conducted on a Bruker D8 Discover diffractometer using Cu K $\alpha$  radiation source ( $\lambda = 1.54$  Å). The step size was 0.01°. A low-voltage scanning electron microscope (FEI Verios 460 XHR) was used to record SEM images. The accelerating voltage was kept at 3 keV to prevent beam damage to the specimens. The haze ratio was calculated as the ratio of the diffused transmittance to the total transmittance, following a method according to the literature.<sup>[61,62]</sup> An integrating sphere was employed to measure spectra of the incident light with/without specimen and the scattered light by the specimen alone or by both the instrument and the specimen.

**Solar Cell Fabrication:** Prepatterned ITO substrates were cleaned by sonication in deionized water, acetone, and isopropyl alcohol, and then dried with nitrogen. For the electron transport layer, diluted SnO<sub>2</sub> dispersion (2 wt% in H<sub>2</sub>O) was spin-coated at 4000 rpm for 30 s and then annealed at 185 °C for 30 min. The substrates were then moved into a vacuum chamber for perovskite layer deposition. The active layer was deposited by thermal co-evaporation of precursors under the conditions described above. Subsequently, the hole transport layer was deposited on top of the active layer by spin-coating a Spiro-OMeTAD solution at 4000 rpm for 30 s. The Spiro-OMeTAD solution was prepared by dissolving the Spiro-OMeTAD in 1 mL chlorobenzene at a concentration of 60 mM, with the addition of 30 mM Li-TFSI from a stock solution in acetonitrile and 200 mM of t-BP. For humidity and high-temperature stability test, the hole-transport layer was deposited on top of the active layer by spin-coating CuSCN solution at 5000 rpm for 60 s, and then the stacks were annealed at 70 °C for 10 min. The CuSCN solution was prepared by dissolving the 30 mg CuSCN in 1 mL diethyl sulfide. Finally, solar cells were completed by either thermal evaporation of 100 nm thick gold, or sputtering 140 nm thick ITO (40 ± 5  $\Omega$  sq<sup>-1</sup>) at a rate of 0.3 Å s<sup>-1</sup> in vacuum (< 2 × 10<sup>-6</sup> mbar). Active areas of 0.09, 1.2, 10, and 25 cm<sup>2</sup> were defined using shadow masks of different sizes.

**Solar Cell Characterization:** TPVs were placed under simulated AM1.5G (100 mW cm<sup>-2</sup>) illumination provided by a 300 W xenon arc lamp (Newport Oriol) without a light aperture in a nitrogen-filled glovebox. The  $J$ - $V$  characteristics were measured without preconditioning by a Keithley 2400 source measurement unit. The scan speed and dwell time were 0.01 V s<sup>-1</sup> and 0.05 s (reverse scan: 1.9—0.1 V, forward scan: -0.1—1.9 V), respectively. The EQE was measured using a lock-in amplifier with chopped, monochromated illumination from a 300 W Xenon arc lamp (Newport Oriol) in ambient environment. A NIST-traceable calibrated photodetector (Newport model 71 582) was used to calibrate the intensities of both the solar simulator and the EQE lamp.

**Stability Measurement Under Continuous Illumination:** Stability studies were conducted according to the ISOS-L-II protocol.<sup>[49]</sup> Devices were encapsulated in a nitrogen glovebox with a cover glass and UV-curable epoxy applied along its perimeter. Devices were illuminated from the glass/cathode side, thus their performance was identical before and after encapsulation. The encapsulated devices were mounted on homebuilt printed circuit boards and connected to a Keithley 2401 and a Keithley 2700 with two 7705 multiplexer units and tested without any additional filters. The devices were aged under continuous illumination from a metal halide lamp. The lamp spectrum, as shown in Figure S11, Supporting Information, was measured by an Ocean Optics spectrometer and was periodically remeasured during the experiment to correct for intensity fluctuation. The devices were mounted to a cold metal plate with chilled water circulating through it to maintain the temperature of solar cells. The temperature of solar cells was measured outside the encapsulation on the surface of the cover glass using a thermocouple.  $J$ - $V$  characteristics were measured every 5 min. The initial values at the MPP were obtained from each  $J$ - $V$  sweep, and then



devices were kept at the MPP during operation by applying an active load developed by infinityPV ApS. During lifetime studies, the devices were also periodically removed for  $J$ - $V$  and EQE measurement at room temperature to cross-calibrate and account for error due to intensity fluctuation of the solar simulator with time.

**Humidity Stability Measurement:** For the humidity stability tests, solar cells were stored in a sealed container at room temperature without encapsulation in the dark. The relative humidity was maintained at  $70 \pm 5\%$  in the container.

**Thermal Stability Measurement:** Unencapsulated solar cells were placed on a hotplate at  $85^\circ\text{C}$  in a nitrogen glovebox in the dark for thermal stability measurement.

**TPV Demonstration:** The ECW was obtained from Ambilight, Inc. The solar cell was mounted on the ECW as a combined stack. The solar cell was electrically connected to the ECW to drive its switching between its colored and bleached states. The connections were reversed to access the bleached state. The digital clock and toy car were also obtained commercially. Two  $25\text{ cm}^2$  TPVs were connected in series to the digital clock to power it. A  $25\text{ cm}^2$  TPV was connected to the toy car with an intermediate voltage regulator.

**Average Visible Transmission Calculation:** The AVT was calculated using

$$\text{AVT} = \frac{\int T(\lambda)P(\lambda)S(\lambda)d(\lambda)}{\int P(\lambda)S(\lambda)d(\lambda)} \quad (1)$$

where  $\lambda$  is the wavelength,  $T$  is transmission,  $P$  is the photopic spectral response of the human eye, and  $S$  is solar irradiance.

## Supporting Information

Supporting Information is available from the Wiley Online Library or from the author.

## Acknowledgements

T.L. thanks the Julis Romo Rabinowitz Graduate Fellowship for funding. Y.-L. Loo acknowledged support from the National Science Foundation, under grants DMR-1627453, CMMI-1824674 and STTR-1843743. Q.C.B. thanks the Arnold and Mabel Beckman Foundation for supporting this work. P.W. and M.C. thank the support from the Yan Huo \*94 Fellowship and Andlinger Center for Energy and the Environment of Princeton University. The authors acknowledge the use of Princeton's Imaging and Analysis Center, which was partially supported by the Princeton Center for Complex Materials, a National Science Foundation (NSF)-MRSEC program (DMR-1420541).

## Conflict of Interest

The authors declare no conflict of interest.

## Data Availability Statement

The data that support the findings of this study are available from the corresponding author upon reasonable request.

## Keywords

color neutrality, inorganic perovskites, stability, thermal evaporation, transparent solar cells

Received: January 31, 2022

Revised: April 11, 2022

Published online:

- [1] C. J. Traverse, R. Pandey, M. C. Barr, R. R. Lunt, *Nat. Energy* **2017**, 2, 849.
- [2] Q. Burlingame, Y.-L. Loo, *Sol. Energy Mater. Sol. Cells* **2021**, 227, 111114.
- [3] N. C. Davy, M. Sezen-Edmonds, J. Gao, X. Lin, A. Liu, N. Yao, A. Kahn, Y.-L. Loo, *Nat. Energy* **2017**, 2, 17104.
- [4] Y. Liu, J. Wang, F. Wang, Z. Cheng, Y. Fang, Q. Chang, J. Zhu, L. Wang, J. Wang, W. Huang, T. Qin, *Nat. Commun.* **2021**, 12, 3360.
- [5] A. Cannavale, M. Hörantner, G. E. Eperon, H. J. Snaith, F. Fiorito, U. Ayr, F. Martellotta, *Appl. Energy* **2017**, 194, 94.
- [6] A. Cannavale, G. E. Eperon, P. Cossari, A. Abate, H. J. Snaith, G. Gigli, *Energy Environ. Sci.* **2015**, 8, 1578.
- [7] F. Martellotta, A. Cannavale, U. Ayr, *Energy Procedia* **2017**, 126, 219.
- [8] M. L. Ball, Q. Burlingame, H. L. Smith, T. Liu, S. R. Parkin, A. Kahn, Y.-L. Loo, *ACS Energy Lett.* **2022**, 7, 180.
- [9] S. Ullbrich, J. Benduhn, X. Jia, V. C. Nikolis, K. Tvingstedt, F. Piersimoni, S. Roland, Y. Liu, J. Wu, A. Fischer, D. Neher, S. Reineke, D. Spoltore, K. Vandewal, *Nat. Mater.* **2019**, 18, 459.
- [10] A. J. Lopez-Garcia, A. Bauer, R. F. Rubio, D. Payno, Z. J. Li-Kao, S. Kazim, D. Hariskos, V. Izquierdo-Roca, E. Saucedo, A. Pérez-Rodríguez, *Sol. RRL* **2020**, 4, 2000470.
- [11] R. Karsthorf, P. Räckle, H. von Wenckstern, M. Grundmann, *Phys. Status Solidi* **2016**, 213, 30.
- [12] M. Warasawa, Y. Watanabe, J. Ishida, Y. Murata, S. F. Chichibu, M. Sugiyama, *Jpn. J. Appl. Phys.* **2013**, 52, 021102.
- [13] K. M. Boopathi, C. Hanmandlu, A. Singh, Y.-F. F. Chen, C. S. Lai, C. W. Chu, *ACS Appl. Energy Mater.* **2018**, 1, 632.
- [14] D. Liu, C. Yang, P. Chen, M. Bates, S. Han, P. Askeland, R. R. Lunt, *ACS Appl. Energy Mater.* **2019**, 2, 3972.
- [15] D. Liu, C. Yang, R. R. Lunt, *Joule* **2018**, 2, 1827.
- [16] G. Liu, C. Wu, Z. Zhang, Z. Chen, L. Xiao, B. Qu, *Sol. RRL* **2020**, 4, 2000056.
- [17] T. Liu, Q. C. Burlingame, J. C. Sorli, M. L. Ball, G. Cheng, N. Yao, Y.-L. Loo, *Adv. Energy Mater.* **2021**, 11, 2100225.
- [18] R. R. Lunt, *Appl. Phys. Lett.* **2012**, 101, 043902.
- [19] J. Werner, J. Geissbühler, A. Dabirian, S. Nicolay, M. Morales-Masis, S. De Wolf, B. Niesen, C. Ballif, *ACS Appl. Mater. Interfaces* **2016**, 8, 17260.
- [20] X. Zhao, L. Tian, T. Liu, H. Liu, S. Wang, X. Li, O. Fenwick, S. Lei, W. Hu, *J. Mater. Chem. A* **2019**, 7, 1509.
- [21] J. A. Raiford, R. A. Belisle, K. A. Bush, R. Prasanna, A. F. Palmstrom, M. D. McGehee, S. F. Bent, *Sustainable Energy Fuels* **2019**, 3, 1517.
- [22] A. Ishii, T. Miyasaka, A. Ishii, T. Miyasaka, *Adv. Sci.* **2020**, 7, 1903142.
- [23] J. Ávila, C. Momblona, P. P. Boix, M. Sessolo, H. J. Bolink, *Joule* **2017**, 1, 431.
- [24] M. Liu, M. B. Johnston, H. J. Snaith, *Nature* **2013**, 501, 395.
- [25] Y. Vaynzof, *Adv. Energy Mater.* **2020**, 10, 2003073.
- [26] L. Gil-Escrig, C. Dreessen, I. C. Kaya, B. S. Kim, F. Palazon, M. Sessolo, H. J. Bolink, *ACS Energy Lett.* **2020**, 5, 3053.
- [27] Y. Xia, R. Li, E. Tsai, Y. He, T. Liu, X. Zhao, K. Gu, H. Meng, Y.-L. Loo, *Adv. Electron. Mater.* **2021**, 2021, 2000792.
- [28] W. Xiang, S. (Frank) Liu, W. Tress, *Energy Environ. Sci.* **2021**, 14, 2090.
- [29] W. Xiang, W. Tress, *Adv. Mater.* **2019**, 31, 1902851.
- [30] T. Liu, X. Zhao, J. Li, Z. Liu, F. Liscio, S. Milita, B. C. Schroeder, O. Fenwick, *Nat. Commun.* **2019**, 10, 5750.
- [31] X. Zhao, C. Yao, T. Liu, J. C. Hamill, G. O. N. Ndjawa, G. Cheng, N. Yao, H. Meng, Y.-L. Loo, *Adv. Mater.* **2019**, 31, 1904494.
- [32] U. Holzwarth, N. Gibson, *Nat. Nanotechnol.* **2011**, 6, 534.
- [33] G. Xia, H. Liu, X. Zhao, X. Dong, S. Wang, X. Li, *Chem. Eng. J.* **2019**, 370, 1111.
- [34] F. Zhang, W. Shi, J. Luo, N. Pellet, C. Yi, X. Li, X. Zhao, T. J. S. Dennis, X. Li, S. Wang, Y. Xiao, S. M. Zakeeruddin, D. Bi, M. Grätzel, *Adv. Mater.* **2017**, 29, 1606806.
- [35] X. Zhao, T. Liu, Y.-L. Loo, *Adv. Mater.* **2022**, 34, 2105849.

- [36] X. Zhao, T. Liu, A. B. Kaplan, C. Yao, Y.-L. Loo, *Nano Lett.* **2020**, *20*, 8880.
- [37] Q. Zhou, J. Duan, X. Yang, Y. Duan, Q. Tang, *Angew. Chem., Int. Ed.* **2020**, *59*, 21997.
- [38] H. Kim, C. M. Gilmore, A. Piqué, J. S. Horwitz, H. Mattoussi, H. Murata, Z. H. Kafafi, D. B. Chrisey, *J. Appl. Phys.* **1999**, *86*, 6451.
- [39] Y. Li, X. Guo, Z. Peng, B. Qu, H. Yan, H. Ade, M. Zhang, S. R. Forrest, *Proc. Natl. Acad. Sci.* **2020**, *117*, 21147.
- [40] J. Meiss, M. K. Riede, K. Leo, *J. Appl. Phys.* **2009**, *105*, 063108.
- [41] Q. Tai, F. Yan, *Adv. Mater.* **2017**, *29*, 1700192.
- [42] J. Werner, G. Dubuis, A. Walter, P. Löper, S. J. Moon, S. Nicolay, M. Morales-Masis, S. De Wolf, B. Niesen, C. Ballif, *Sol. Energy Mater. Sol. Cells* **2015**, *141*, 407.
- [43] H. Kanda, A. Uzum, A. K. Baranwal, T. A. N. Peiris, T. Umeyama, H. Imahori, H. Segawa, T. Miyasaka, S. Ito, *J. Phys. Chem. C* **2016**, *120*, 28441.
- [44] H. Wang, H. A. Dewi, T. M. Koh, A. Bruno, S. Mhaisalkar, N. Mathews, *ACS Appl. Mater. Interfaces* **2020**, *12*, 484.
- [45] Q. Jiang, X. Zhang, J. You, *Small* **2018**, *14*, 1801154.
- [46] P. Qi, F. Zhang, X. Zhao, X. Liu, X. Bi, P. Wei, Y. Xiao, X. Li, S. Wang, *Energy Technol.* **2017**, *5*, 1173.
- [47] X. Zhao, F. Zhang, C. Yi, D. Bi, X. Bi, P. Wei, J. Luo, X. Liu, S. Wang, X. Li, S. M. Zakeeruddin, M. Grätzel, *J. Mater. Chem. A* **2016**, *4*, 16330.
- [48] F. Zhang, X. Zhao, C. Yi, D. Bi, X. Bi, P. Wei, X. Liu, S. Wang, X. Li, S. M. Zakeeruddin, M. Grätzel, *Dyes Pigm.* **2017**, *136*, 273.
- [49] M. V. Khenkin, E. A. Katz, A. Abate, G. Bardizza, J. J. Berry, C. Brabec, F. Brunetti, V. Bulović, Q. Burlingame, A. Di Carlo, R. Cheacharoen, Y.-B. Cheng, A. Colmann, S. Cros, K. Domanski, M. Duszka, C. J. Fell, S. R. Forrest, Y. Galagan, D. Di Girolamo, M. Grätzel, A. Hagfeldt, E. von Hauff, H. Hoppe, J. Kettle, H. Köbler, M. S. Leite, S. Liu, Y.-L. Loo, J. M. Luther, et al., *Nat. Energy* **2020**, *5*, 35.
- [50] S. Bai, P. Da, C. Li, Z. Wang, Z. Yuan, F. Fu, M. Kawecki, X. Liu, N. Sakai, J. T. W. Wang, S. Huettnner, S. Buecheler, M. Fahlman, F. Gao, H. J. Snaith, *Nature* **2019**, *571*, 245.
- [51] X. Zhao, C. Yao, K. Gu, T. Liu, Y. Xia, Y.-L. Loo, *Energy Environ. Sci.* **2020**, *13*, 4334.
- [52] "PVWatts Calculator," can be found under <https://pvwatts.nrel.gov/pvwatts.php>, n.d.
- [53] L. Yang, W. L. Tsai, C. S. Li, B. W. Hsu, C. Y. Chen, C. I. Wu, H. W. Lin, *ACS Appl. Mater. Interfaces* **2019**, *11*, 47054.
- [54] X. Li, B. He, Z. Gong, J. Zhu, W. Zhang, H. Chen, Y. Duan, Q. Tang, *Sol. RRL* **2020**, *4*, 2000362.
- [55] J. Liang, C. Wang, Y. Wang, Z. Xu, Z. Lu, Y. Ma, H. Zhu, Y. Hu, C. Xiao, X. Yi, G. Zhu, H. Lv, L. Ma, T. Chen, Z. Tie, Z. Jin, J. Liu, *J. Am. Chem. Soc.* **2016**, *138*, 15829.
- [56] Q. Tai, K. C. Tang, F. Yan, *Energy Environ. Sci.* **2019**, *12*, 2375.
- [57] S. Sanchez, N. Christoph, B. Grobety, N. Phung, U. Steiner, M. Saliba, A. Abate, *Adv. Energy Mater.* **2018**, *8*, 1802060.
- [58] X. Zhao, T. Liu, W. Shi, X. Hou, T. J. S. Dennis, *Nanoscale* **2019**, *11*, 2453.
- [59] M. Z. Li, C. C. Lee, S. Biring, I. S. Hsu, D. Luo, R. Estrada, Y. S. Wu, C. C. Yang, S. W. Liu, *Sol. RRL* **2021**, *5*, 2000564.
- [60] J. Li, H. Wang, X. Y. Chin, H. A. Dewi, K. Vergeer, T. W. Goh, J. W. M. Lim, J. H. Lew, K. P. Loh, C. Soci, T. C. Sum, H. J. Bolink, N. Mathews, S. Mhaisalkar, A. Bruno, *Joule* **2020**, *4*, 1035.
- [61] J. Wang, C. Meng, Q. Gu, M. C. Tseng, S. T. Tang, H. S. Kwok, J. Cheng, Y. Zi, *ACS Nano* **2020**, *14*, 3630.
- [62] F. Galeotti, W. Mróz, M. Catellani, B. Kutrzeba-Kotowska, E. Kozma, *J. Mater. Chem. C* **2016**, *4*, 5407.